SPECTRAL PROPERTIES OF Eu^{3+} AND RHODAMINE 6G EMITTERS IN OPAL PHOTONIC CRYSTAL FILMS

V. S. Mukharovska*, M. P. Derhachov, V. M. Moiseyenko

Oles Honchar Dnipro National University, Dnipro, Ukraine
**e-mail: muhar10518@gmail.com*

The Eu^{3+} photoluminescence spectra measured on the infiltrated opal film areas with visible structural defects are found to be independent of the observation angle and essentially different from the Eu^{3+} spectrum obtained on the visually homogeneous film areas. This is explained in the framework of the multi-site occupation model where the defect boundaries facilitate the stabilization of specific coordination environment of the Eu^{3+} ions. A sandwich-like geometry of opal films is found to provide optical feedback for rhodamine 6G, resulting in significant spectral modification and intensity enhancement. It is shown that these changes are not caused by concentration or thermal gradients.

Keywords: opal film, photoluminescence, optical feedback, europium ions, rhodamine 6G.

Received 29.10.2025; Received in revised form 27.11.2025; Accepted 10.12.2025

1. Introduction

Modern optoelectronics requires advanced materials to manipulate the spectral and spatial distribution of radiation. One of the leading solutions in this area is photonic crystals (PhCs), artificial periodic structures with a refractive index modulation scale comparable to the light wavelength. Their defining feature is the formation of spectral range, called the photonic band gap or the photonic stop band (PhSB), where photon propagation is inhibited due to destructive interference [1]. Among the diverse PhC architectures, opal films occupy a noticeable position. Their planar geometry, combined with a relatively low defect density and rapid fabrication process [2], makes them a highly promising platform for the next-generation optical devices. Beyond fundamental research, they have found extensive applications in optical filtering [3], sensors [4], solar energy [5], reflective displays [6], and anti-counterfeiting [7].

Furthermore, the utilization of PhCs opens broad horizons for the design of novel laser sources [8]. Depending on the degree of structural order, such systems can support distinct light generation mechanisms. In disordered media, multiple scattering can provide the necessary feedback for random lasing [9]. Conversely, in highly ordered structures, the periodic lattice itself acts as a distributed feedback resonator enabling classical laser action. A significant advantage of opal films lies in their versatility offering a single material platform capable of realizing both lasing regimes.

Earlier, we have examined the effects of photonic stop band [10] and local coordination environment [11] on the Eu^{3+} emission spectrum in single opal films and heterostructures. In this work, we investigate the influence of macroscopic defects and optical feedback on the spectral characteristics of laser-active media such as europium (III) acetate hydrate and rhodamine 6G in synthetic opal films.

2. Experimental technique

Monodisperse spherical silica particles were synthesized via the modified Stöber-Fink-Bohn technique involving the hydrolysis of tetraethyl orthosilicate in an ethanol-ammonia medium [12]. The diameter of particles was controlled by adjusting the concentration ratio of the reaction components. The particles were subsequently self-assembled into ordered opal films on glass substrates by using the method of vertically moving meniscus driven by the evaporative deposition. The grown opal films were annealed at 450 °C to eliminate organic residues and adsorbed water. The opal structure was assumed to be a face-centred cubic (fcc) lattice with the plane (111) parallel to the film surface [13].

The samples with the Eu^{3+} ions were obtained by impregnating original opal films with a saturated aqueous solution of europium (III) acetate hydrate $Eu(CH_3COO)_3 \cdot xH_2O$ with the following drying at room temperature. For the laser dye experiments, a sandwich-like cavity was constructed using two opal films on glass substrates, mechanically pressed to ensure parallelism of the planes (111) of the fcc lattice. An ethanol solution with a rhodamine 6G (R6G) concentration of 10^{-4} M was used to fulfil the inter-film space.

Photoluminescence (PL) measurements were performed at room temperature using a modified laser spectrometer based on a double monochromator DFS-12 with a photon counting system. The spectral resolution was maintained at 0.5 cm^{-1}. The emission of Eu^{3+} ions was excited by a 410 nm semiconductor laser radiation (targeting the $^5L_6 \leftarrow {}^7F_1$ and $^5L_6 \leftarrow {}^7F_0$ transitions). Measurements were performed in a forward scattering geometry at various observation angles relative to the [111] axis, the normal to the film surface. For the R6G emission investigations, a 532 nm diode-pumped solid-state laser was used. The position of the excitation spot relative to the sample edge was precisely controlled using a micrometric stage, and the PL spectra were registered from the end face of the cell in a right-angle scattering geometry.

3. Results and discussion

The PL spectrum measured on a visually homogeneous, macroscopic defect-free area of the infiltrated opal film is similar to the spectrum of the $Eu(CH_3COO)_3 \cdot xH_2O$ salt in a 'free state' in an optical cell (curve 1 in Fig. 1). It shows only the angle-dependent intensity modulation due to the PhSB effect, as described in paper [10]. In contrast, the spectra measured on the film areas with visible structural defects (film breaks and cracks) are strongly different both from the reference spectrum and to each other (curves 2 and 3 in Fig. 1). Furthermore, they remain unchanged when the viewing angle is altered, eliminating the PhSB effect as a cause of such changes. Instead, we can consider the structural defects as optical cavities that concentrate external electromagnetic field with raising its impact on the Eu^{3+} ions localized within these structural irregularities. In this case, it is reasonable to assume that structural defects act like optical cavities that concentrate the external electromagnetic field amplifying its effect and resulting in the rebuilding of the spectrum of Eu^{3+} ions located in these irregularities.

Detailed analysis of the forbidden $^5D_0 \rightarrow {}^7F_0$ transition reveals that Eu^{3+} ions occupy multiple non-equivalent sites specifically within the defect volume. Since the non-degenerate $J = 0$ levels cannot undergo Stark splitting, the observed multi-peak structure serves as a direct probe for site multiplicity. We identify at least two such sites for point 1 (curve 2 in Fig. 1) and four ones for point 2 (curve 3 in Fig. 1), characterized by the difference of $\Delta E \approx 41$ cm^{-1} and 65 cm^{-1}, respectively. Such large energy differences are typically indicative of distinct geometrical isomers [14]. The absence of the resolved fine structure of the $^5D_0 \rightarrow {}^7F_0$ transition in defect-free film areas, where the emission represents a bulk-averaged environment, suggests that the structural imperfections create distinct local environments. It is plausible that the defect boundaries facilitate the stabilization of specific coordination geometries that are otherwise statistically insignificant in the defect-free opal matrix.

The reasonability of interpreting the observed changes within the framework of the multi-site occupation model is further corroborated by the splitting pattern of the magnetic dipole transition $^5D_0 \rightarrow {}^7F_1$. Based on the selection rules for magnetic dipole transitions, the maximum number of the Stark components should be three. The experimental data exceeds this theoretical limit for a single position: four emission lines are observed for point 1, and eight ones for point 2. This multiplicity is explicable only as a superposition of the Stark patterns from the non-equivalent sites identified in the $^5D_0 \rightarrow {}^7F_0$ region. Moreover, the total

Stark splitting of the F_1 manifold for point 2 reaches approximately 340 cm^{-1}. Such a value suggests that the ions trapped at the defect interface might be subjected to a crystal field of significant strength [14], potentially exceeding that experienced by ions in the bulk opal.

Finally, we analyzed the intensity ratio $R = I(^5D_0 \rightarrow {}^7F_2)/I(^5D_0 \rightarrow {}^7F_1)$. Although frequently utilized as a direct metric for site asymmetry, it is important to consider that the intensity of this hypersensitive transition $^5D_0 \rightarrow {}^7F_2$ is fundamentally governed by the nature of the ligands and the specific parameters of the ligand field, rather than geometric distortion alone [14]. The value of the ratio for point 1 ($R \approx 1.74$) is comparable to that for the bulk salt ($R \approx 1.53$). In contrast, for point 2 we have a significantly reduced ratio of $R \approx 0.97$. Since the intense and split $^5D_0 \rightarrow {}^7F_0$ transition already precludes the presence of a center of inversion, this anomalous decrease in R implies a specific modification of the local crystal field potential. It is plausible to assume that the rigid walls of the defect impose a specific coordination geometry that alters the crystal field parameters acting on the ion, thereby suppressing the electric dipole transition probability despite the low site symmetry.

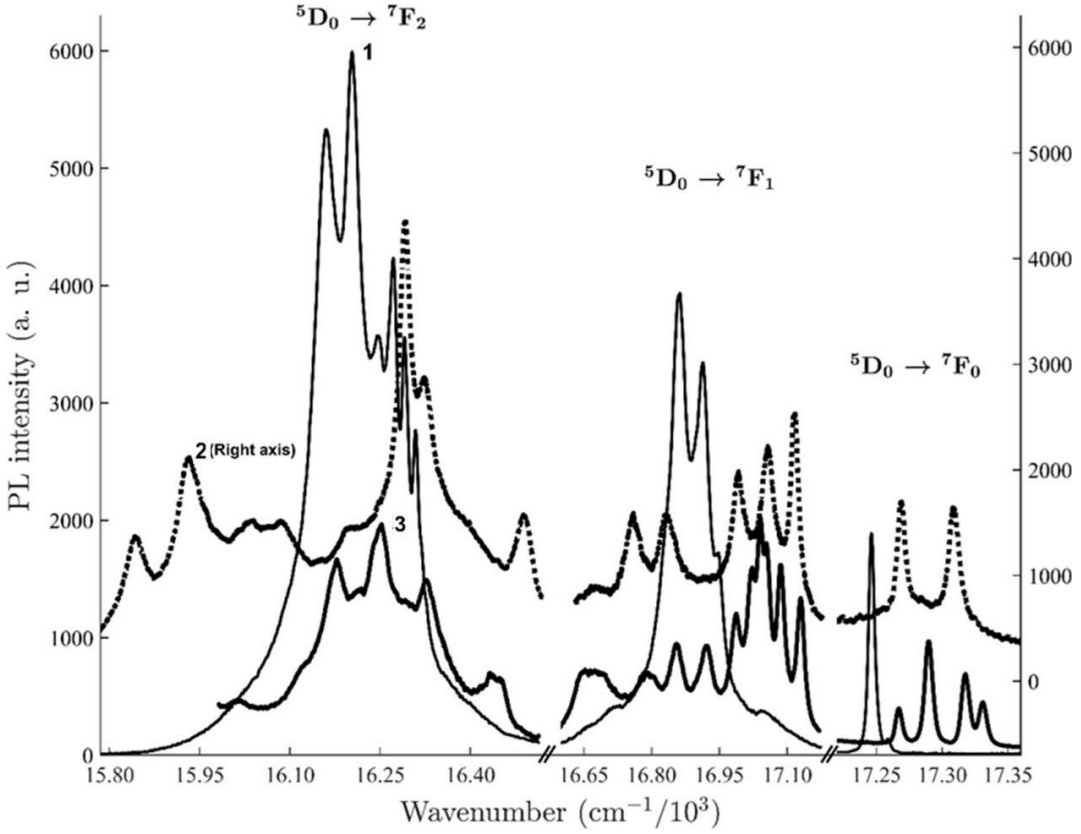

Fig. 1. PL Eu^{3+} spectrum measured in an optical cell (1, $Eu(CH_3COO)_3 \cdot xH_2O$) and in different points of opal film near macroscopic structural defects (2, 3). The Eu^{3+} spectrum measured in the defect-free opal region has a profile similar to the curve 1.

In the second part of the paper, we discuss the emission features of R6G molecules incorporated into resonant-type photonic crystal structures. A distinct experimental geometry for measurements of the R6G PL spectra is inserted in the top right corner of Fig. 2. The ethanol-based R6G solution was infiltrated into a 0.24 mm vertical space defined by two parallel opal photonic crystal films creating a sandwich-like structure, with the space

thickness maintained by mica spacers. The PL spectrum was taken from the end face when the solution was illuminated by both unfocused and focused laser beams near the end face (point A) and far from the edge (point C), as schematically illustrated in the insert of Fig. 2.

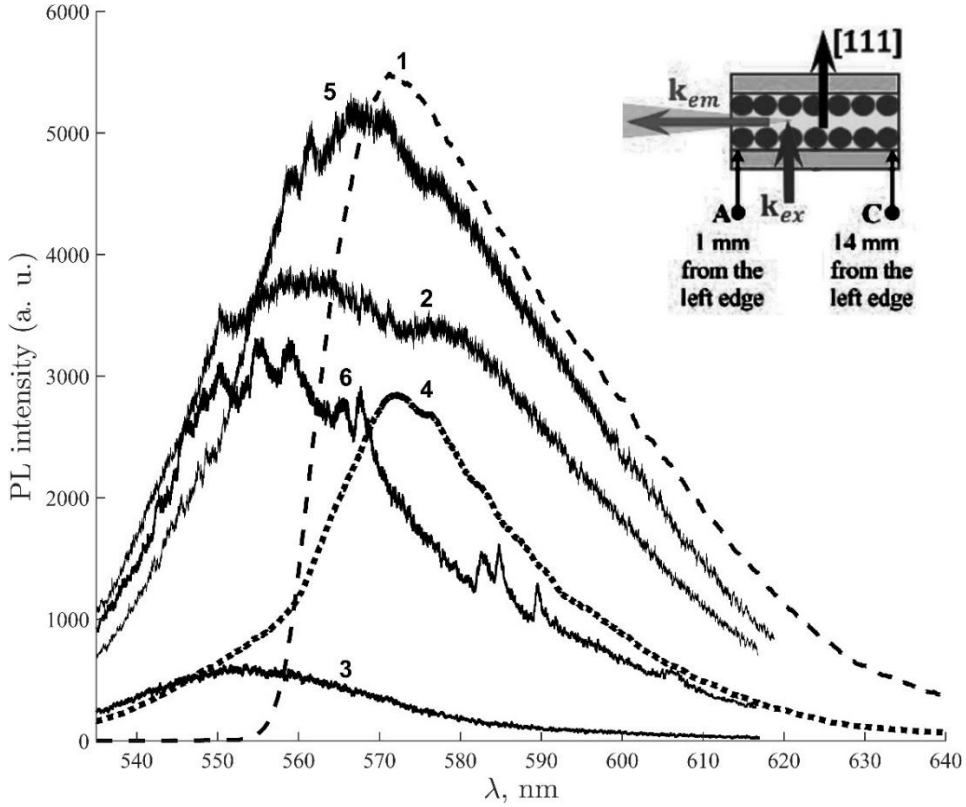

Fig. 2. PL spectra of the R6G solution in an optical cell (1), in a sandwich-like structure under excitation in point C (2) by focused laser beam and in point A by unfocused (4) and focused (5) laser beam, as well as under excitation in the vicinity of point C (3) and point A (6) where glass substrate areas are free from the opal film. The curve 6 is multiplied by a factor of 1.25.
The insert illustrates the experimental geometry (top view), indicating the excitation (k_{ex}) and emission (k_{em}) wave vectors, as well as the positions of the excitation points A and C.

Unfocused excitation yielded a broad, smooth, blue-shifted emission band (curve 4 in Fig. 2). The 'blue shift' of the R6G emission band is primarily explained by the waveguiding properties of the sandwich-like structure, specifically by increasing the number of higher energy photons along the registration axis. When emitted in the solution, such photons falling at larger angles onto an opal film may undergo reflection in the spectral region of the PhSB, shifted to the 'blue' side for these angles of incidence. To exclude the opal film effect on the PL spectrum, the excitation was also performed in the vicinity of points A and C, where the glass substrate areas were free of the opal film. These spectra (curves 3 and 6 in Fig. 2) contained similar modes (suggesting a Fabry-Perot cavity effect), but they were attenuated and not resolved far from the edge, in point C. The photonic crystal structure, however, resolves these modes even at point C. This implies that the photonic crystal structure provides feedback or guidance that enhances the propagation of these resonant modes at high excitation density.

We also considered whether these spectral features stem from physicochemical changes in the dye solution. Indeed, a decrease in effective dye concentration leads to a blueshift by

favoring monomer emission [15]. Similarly, local laser heating could contribute to a hypsochromic shift via the thermo-optic effect [16]. However, comparative analysis between the glass and opal substrates rules these out as primary mechanisms. First, the emission on original glass exhibits the largest overall blue shift, yet its peak position remains identical between the edge (point A) and the interior (point C). This spatial stability indicates that no significant concentration or thermal gradients exist to alter the emission profile over distance. In contrast, the opal structure exhibits a dynamic evolution: the spectrum under excitation at point C is more strongly 'blue-shifted' than that under excitation at point A. Furthermore, the emission intensity in the opal structure is notably higher than in the glass control for both cases. If the mechanism were purely passive scattering or absorption, the intensity on the porous opal film would likely be lower. The observed intensity enhancement combined with the spatial mode preservation confirms that the photonic crystal effectively confines the emission, channeling it along the detection axis via a structural waveguiding mechanism.

4. Conclusions

The scanning of the surface of opal film infiltrated with europium (III) acetate hydrate $Eu(CH_3COO)_3 \cdot xH_2O$ reveals the existence of surface areas characterized by significant spectral modification. These surface areas contain structural defects visible to the naked eye, and the changes themselves are manifested in redistribution of spectral intensity and an increase in the number of the Eu^{3+} emission bands. Since these observed spectra do not undergo any changes when the observation angle is altered, their difference from the spectra measured on the visually homogeneous, 'defect-free' surface areas cannot be adequately interpreted only by the influence of the photonic stop band. In this case, it is most reasonable to assume the rearrangement of the Eu^{3+} energy spectrum in the vicinity of the structural defects. This may be due to both the external electromagnetic field concentrated on structural defects, acting like optical cavities, and the formation of several stable configurations of the Eu^{3+} environment, which differ from those in 'defect-free' volume of the film. Analysis of the number of the observed emission lines in the magnetic dipole transition $^5D_0 \rightarrow {}^7F_1$ region and the values of intensity ratio $R = I(^5D_0 \rightarrow {}^7F_2)/I(^5D_0 \rightarrow {}^7F_1)$ testifies a dominant role of the specific coordination geometries in the Eu^{3+} environment on the defect boundaries.

In contrast to the situation just discussed above, changes in the spectrum of R6G molecules inside resonant-type structures are mainly caused by the PhSB effect. As known, at larger angles θ of incidence, the reflectivity of the opal film with an averaged permittivity ε_{av} increases for the higher energy photons, in accordance with the expression for the spectral position λ_c of the PhSB center $\lambda_c = 2\, d_{111}\sqrt{\varepsilon_{av} - \sin^2\theta}$, where d_{111} is the distance between the planes (111). In case of the right-angle geometry (the insert in Fig. 2), it results in raising the number of photons in the viewing direction, similar to the waveguide effect. In addition, the comparison of the spectra under excitation in the surface areas with and without opal film let us suppose that the concentration and thermal gradients in the solution are practically absent and do not affect the spectral distribution in the photoluminescence spectrum of R6G molecules in sandwich-like cavity formed by two opal films.

References

1. **Joannopoulos, J. D.** Molding the flow of light / J. D. Joannopoulos, S. G. Johnson, J. N. Winn, R. D. Meade // Princet. Univ. Press (Princeton, NJ). – 2008.

2. **Muldarisnur, M.** Structure and optical properties of opal films made by an out-of-plane electric field-assisted capillary deposition method / M. Muldarisnur, F. Marlow // ACS Omega. – 2022. – Vol. 7. – P. 8084 – 8090. doi.org/10.1021/acsomega.1c07391

3. **Shalaev, M.** Optically tunable topological photonic crystal / M. Shalaev, W. Walasik, N. M. Litchinitser // Optica. – 2019. – Vol. 6, Issue 7. – P. 839 – 844. doi.org/10.1364/optica.6.000839

4. **Li, T.** Recent advances in photonic crystal-based sensors / T. Li, G. Liu, H. Kong, G. Yang, G. Wei, X. Zhou // Coord. Chem. Rev. – 2023. – Vol. 475. – P. 21 – 31. doi.org/10.1016/j.ccr.2022.214909

5. **Guo, S.** Unidirectional ultrabroadband and wide-angle absorption in graphene-embedded photonic crystals with the cascading structure comprising the Octonacci sequence / S. Guo, C. Hu, H. Zhang // J. Opt. Soc. Am. B. – 2020. – Vol. 37(9). – P. 2678 – 2687. doi.org/10.1364/josab.399048

6. **Kim, D. Y.** Stretchable and reflective displays: materials, technologies and strategies / D. Y. Kim, M. J. Kim, G. Sung, J. Y. Sun // Nano. – 2019. – Vol. 6. – P. 21. doi.org/10.1186/s40580-019-0190-5

7. **Winter, T.** Dye-loaded mechanochromic and pH-responsive elastomeric opal films / T. Winter, A. Boehm, V. Presser, M. Gallei // Macromol. Rapid Commun. – 2021. – Vol. 42. – P. 7. doi.org/10.1002/marc.202000557

8. **Lonergan, A.** Many Facets of Photonic Crystals: From Optics and Sensors to Energy Storage and Photocatalysis / A. Lonergan , C. O'Dwyer // Advanced Materials Technologies. – 2022. – Vol. 8. – P. 1 – 47. doi.org/10.1002/admt.202201410

9. **Alimov, O. K.** Conversion of the luminescence of laser dyes in opal matrices to the stimulated emission / O. K. Alimov, T. T. Basiev, Y. V. Orlovskii, V. V. Osiko, M. I. Samoilovich // Quantum Electron. – 2008. – Vol. 38. – P. 665. doi.org/10.1070/qe2008v038n07abeh013714

10. **Mukharovska, V. S.** Peculiarities of Eu^{3+} photoluminescence in opal photonic crystal films and heterostructures based on them / V. S. Mukharovska, M. P. Derhachov, V. M. Moiseyenko, B. Abu Sal // Ukr. J. Phys. – 2023. – Vol. 68, No. 12. – P. 785. doi.org/10.15407/ujpe68.12.785

11. **Moiseyenko, V. M.** Influence of coordination environment and dielectric contrast on the spectral-luminescent properties of europium ions in the pores of film opals / V. M. Moiseyenko, V. R. Gavrilyak, M. P. Derhachov, V. S. Mukharovska // J. Phys. Electron. – 2022. – Vol. 30. – P. 49 – 54. doi.org/10.15421/332218

12. **Stöber, W.** Controlled growth of monodisperse silica spheres in the micron size range / W. Stöber, A. Fink, E. Bohn // J. Colloid Interface Sci. – 1968. – Vol. 26. – P. 62 – 69. doi.org/10.1016/0021-9797(68)90272-5

13. **Baryshev, A. V.** Photonic band-gap structure: From spectroscopy towards visualization / A. V. Baryshev, A. A. Kaplyanskii, V. A. Kosobukin, [et al.] // Phys. Rev. B. – 2004. – Vol. 70. – P. 113104. doi.org/10.1103/PhysRevB.70.113104

14. **Binnemans, K.** Interpretation of europium(III) spectra / K. Binnemans // Coord. Chem. Rev. – 2015. – Vol. 295. – P. 1 – 45. doi.org/10.1016/j.ccr.2015.02.015

15. **Barzan, M.** Investigation the concentration effect on the absorption and fluorescence properties of Rhodamine 6G dye / M. Barzan, F. Hajiesmaeilbaigi // Optik (Stuttg). – 2018. – Vol. 159. – P. 157 – 161. doi.org/10.1016/j.ijleo.2018.01.075

16. **Bulavin, L. A.** Specific effect of microwaves on the aqueous solution of rhodamine 6G according to fluorescence analysis / L. A. Bulavin, N. V. Gaiduk, M. O. Redkin, A. V. Yakunov // Ukr. J. Phys. – 2021. – Vol. 66. – P. 256. doi.org/10.15407/ujpe66.3.265